

He-atom scattering study of the temperature-dependent charge-density-wave surface structure and lattice dynamics of $2H\text{-TaSe}_2(001)$

G. Brusdeylins, C. Heimlich, J. G. Skofronick,* J. P. Toennies, and R. Vollmer
Max-Planck-Institut für Strömungsforschung, D-3400 Göttingen, Federal Republic of Germany

G. Benedek and L. Miglio
Dipartimento di Fisica dell'Università degli Studi di Milano, via Celoria 16, I-20133 Milano, Italy
 (Received 28 August 1989)

Elastic and inelastic He-atom scattering has been used to measure the surface structure and surface dynamics of the layered transition-metal dichalcogenide $2H\text{-TaSe}_2(001)$ crystal. The results cover temperatures from 60 to 140 K. Below $T_0 = 122$ K an incommensurate charge-density wave (CDW) is formed, which becomes commensurate below approximately 90 K. The measured intensities of the CDW diffraction peaks continuously increase with decreasing temperature below 122 K. From the diffraction intensities, the temperature-dependent amplitude of the surface potential corrugation is determined. The corrugation amplitude is used as an order parameter and from its temperature dependence, on cooling, a critical exponent of $\beta = 0.33$ is extracted. Time-of-flight spectra are used to determine the surface-phonon dispersion curves. Although the spectra are nearly the same at 60 and 140 K, a softening in the Rayleigh mode is observed for intermediate temperatures (around 110 K) at $Q = 0.53 \text{ \AA}^{-1}$, which is near the middle of the Brillouin zone. The difference between the bulk and the surface dynamics is interpreted through the use of the dispersive linear-chain model.

I. INTRODUCTION

A systematic experimental effort has been made to study the surface structure and dynamics of layered crystals by He-atom elastic and inelastic scattering (HAS). In the first study in this series the surface-phonon dispersion curves for the hexagonal-close-packed GaSe(001) surface were measured and compared to predictions based on neutron measurements of the bulk.¹ Although the surface dynamics was expected to be very similar to that of the bulk because of the nearly-two-dimensional nature of this layered crystal, the experiments revealed that the bulk and surface dynamics are considerably different. At the surface both the acoustic- and optical-phonon dispersion curves reveal a softening compared to the bulk dispersion curves. A dispersive linear-chain model was subsequently developed to determine how much the bulk force constants needed to be perturbed in order to reproduce the measured surface results.^{1,2} The surface of graphite was studied next by this group, and because of the high phonon energy in graphite (001), only acoustic modes were measured by HAS.³ The Rayleigh mode and the longitudinal surface mode follow essentially the corresponding bulk band edges. However, in a recent repeat of the graphite measurements it was observed that the mode labeled S_7 in Ref. 3 could not be reproduced.⁴ The new results will be presented in a future paper.⁵ Electron-energy-loss spectroscopy (EELS) measurements of the optical modes seems to agree with the corresponding bulk band edges.⁶

We now have focused our interest on the layered dichalcogenides such as TaSe_2 and TaS_2 , the former being

the topic of this paper. In general, these materials have a normal phase at high temperatures, but they undergo a phase transition to a modulated incommensurate phase by forming a charge-density wave at a certain transition temperature T_0 . At an even lower temperature this incommensurate phase may undergo a further phase transition to a commensurate phase where the modulation wave vector is a (small) rational fraction of the lattice vector.⁷ For the individual kinds of the dichalcogenides there may be additional phases in between.

The dichalcogenide crystal consists of hexagonal-close-packed sheets of metal atoms and sheets of group-VI atoms with the metal atoms sandwiched between two sheets of chalcogenides to form a layer. Because the layers are only weakly bonded to each other, they form a nearly-two-dimensional material. These layers can stack differently depending on their preparation and this leads to different polytypes. The simplest polytype is the $1T$ modification, where all sandwiches stack identically on each other. In the experiment reported in this work, we use the $2H$ modification of TaSe_2 , where the unit cell consists of six atoms and spans two layers (Fig. 1). There are large differences between these modifications in electronic and structural properties. For example, the amplitudes of the charge-density wave in the reconstructed phase are much larger in the $1T$ modification than in the $2H$ modification. The group-VI atoms (S or Se) play only a minor role.⁷ For the surface, this has been demonstrated by HAS (Refs. 8–11) and later by the scanning tunneling microscope (STM) technique.¹² The HAS results show for the commensurate phase of $1T\text{-TaS}_2(001)$ that the superlattice diffraction peaks originating from the CDW

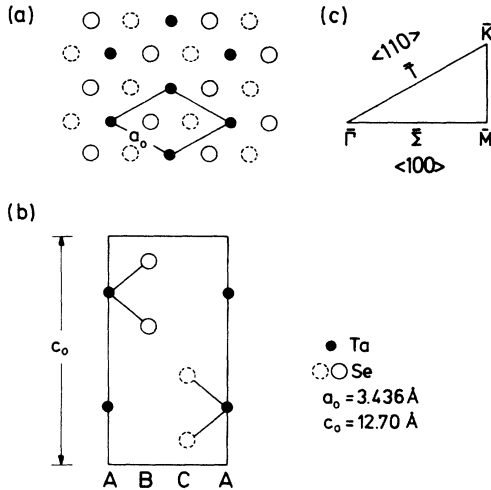


FIG. 1. Crystal structure of $2H\text{-TaSe}_2$ (Ref. 14). (a) Atomic arrangement of the atoms in the unit cell as seen from above, (b) side view, and (c) high-symmetry directions forming an irreducible segment of the surface Brillouin zone.

are as intense as the main Bragg diffraction peaks.^{8,9} In comparison, for $2H\text{-TaSe}_2(001)$ the superlattice diffraction peaks are about 1% of the main Bragg peaks. Thus the phonon branches, which originate from a superlattice peak, are observable in the case of $1T\text{-TaS}_2$ (Ref. 13), but not for $2H\text{-TaSe}_2$ because they are beyond the intensity resolution of our instrument.

The present paper is devoted to the (001) surface of $2H\text{-TaSe}_2$. The phase diagram for bulk $2H\text{-TaSe}_2$ (Fig. 2) shows that the critical temperatures and the observable CDW phases depend on the temperature treatment of the crystal. The striped incommensurate phase (S) can only

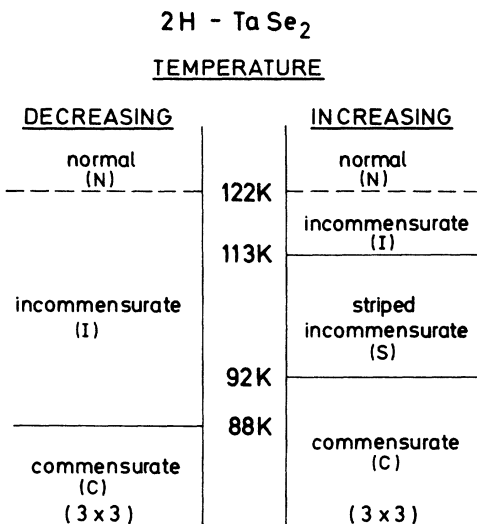


FIG. 2. Phase diagram of $2H\text{-TaSe}_2(001)$ (Ref. 20). The observable phases and the critical temperatures of the phase transitions are dependent on the previous thermal treatment of the crystal.

be observed by warming up the crystal from the low-temperature commensurate phase (C). In the C phase, the induced reconstruction of the crystal leads to a (3×3) superlattice, which is attributed to three CDW's with commensurate wave vectors rotated by 120° with respect to each other.⁷ The different kinds of CDW phases and the critical temperature of the transition ($T_0 = 122 \text{ K}$) from the normal (N) to the fully incommensurate (I) CDW phase have been verified by many different experiments and probes.^{14–29} The I phase is characterized also by three CDW's with wave vectors which are slightly different from the commensurate ones. Three CDW's are also present in the S phase, but here one wave vector is commensurate while the other two are incommensurate. The corresponding striped patterns were first observed by high-resolution electron microscopy.^{30,31} The N-I phase transition is driven by a softening of the longitudinal-acoustic mode around $\frac{2}{3}$ of the Brillouin zone in the $\langle 100 \rangle$ directions. Therefore the displacement pattern in the I phase is just that of the longitudinal mode at that wave vector. A figure of the displacement pattern is shown in Ref. 14.

From the He-atom angular distribution along the $\langle 100 \rangle$ direction, the intensities of the main Bragg peaks and the temperature dependence of the superstructure peaks due to the charge-density wave below 122 K have been determined. For the N phase at $T = 140 \text{ K}$, we have measured the surface-phonon dispersion curves in both the $\langle 100 \rangle$ and $\langle 110 \rangle$ directions and we compare the surface modes with the bulk data reported by Moncton *et al.*¹⁴ Compared to GaSe, the $2H\text{-TaSe}_2$ dispersion curves are much closer to the band edges of the bulk, but still show interesting anomalies originating at the surface. In the $\langle 100 \rangle$ direction at 60 K in the C phase, the Rayleigh mode shows a small deviation with respect to the 140-K dispersion curve in a limited Q -vector range around one-half of the Brillouin zone. Because of this, a carefully controlled temperature-dependence study of the Rayleigh-mode behavior was carried out in this region over the temperature range from 50 to 300 K.

The remainder of this paper is organized as follows. Section II describes the experimental arrangement and the target preparation. In Sec. III, the experimental results are presented and discussed. Finally, in Sec. IV we review the theoretical situation. The paper concludes with a discussion of the implication of this study and surveys the remaining problems.

II. EXPERIMENT

The scattering apparatus has been described previously.^{1,32} The supersonic helium beam is produced in a high-pressure nozzle ($10 \mu\text{m}$ diam) which can be heated to 380 K and cooled to 55 K by a closed-cycle refrigerator. In this way, beam energies between 12 meV ($k_i = 4.8 \text{ \AA}^{-1}$) and 82 meV ($k_i = 12.6 \text{ \AA}^{-1}$) are available. In most of our measurements we use a helium beam with an incident energy of $E_i = 71.5 \text{ meV}$ ($k_i = 11.7 \text{ \AA}^{-1}$). The corresponding stagnation pressures range from 60 to 400 bars, respectively, to assure a velocity spread [full width at half maximum (FWHM)] $\Delta v/v$ of about 1% over the

entire range of stagnation temperatures. The overall regular resolution of the apparatus is about 0.3° . The mass-spectrometer detector views the surface at an angle of 90° with respect to the incident-beam direction. To change the incident angle, the crystal is rotated around an axis perpendicular to the scattering plane.

Altogether, 25 different crystal samples, typically with an area of several mm^2 , and up to 1 mm thick, were tried in this work. The first samples were cleaved in air by the standard sticky-tape technique described in an earlier paper.³ However, nearly all of the work described in this paper was based on measurements made on one crystal which was cleaved in vacuum as described below. Of the other samples, only two, both cleaved in air, gave reasonably sharp diffraction peaks so that a series of measurements could be made.³³ The other samples were poor cleaves with marginal scattered intensity and did not provide useful data. There were no significant differences in the measurements for crystals produced with the two different preparation methods.

For cleaving in vacuum, one side of the sample was first mounted on a stainless-steel holder by a conducting epoxy glue.³⁴ On the other surface, a small lever of glass was glued. In vacuum the crystal was then cleaved by pushing the glass lever against a fixed support inside the chamber. Before cleavage the vacuum system was baked at approximately 100°C for 20 h and before every series of measurements the crystal was heated to 150°C . Higher temperatures were avoided to prevent damage to the crystal. The background pressure in the scattering

chamber was about 10^{-10} Torr. To further reduce residual-gas contamination, the target was surrounded by a liquid-nitrogen cold shield. The mass-spectrometer detector chamber had a background pressure of 4×10^{-11} Torr, mostly due to hydrogen. The He partial pressure was estimated to be approximately only 5×10^{-15} Torr, which gave a background count at mass 4 of about 30 counts/sec. At the specular peak the He signal was about 2×10^6 counts/sec. Near the specular peak the inelastic time-of-flight (TOF) signal was typically 10^3 counts/sec for the best target and depended somewhat on target temperature and beam conditions. At the Brillouin-zone edge, the inelastic count rate was much smaller, and only about 30 counts/sec above the background.

Temperature regulation at the target was improved with respect to previous measurements^{1,32} by using a Ni-Cr/Ni thermocouple in a computer-controlled feedback system which regulated the heating of the target against the cooling produced by liquid nitrogen or liquid helium in the range 50–140 K. The uncertainty in temperature was about ± 0.5 at 300 K and ± 2 K at 60 K, respectively, whereas the temperature fluctuations, as measured by the thermocouple, could be stabilized to ± 0.3 K.

At 140-K target temperature, there was no change in the specular intensity over periods of 10–14 h. However, when the target was at 60 K, the signal dropped by about 25% over the same period, but then returned to its original strength after a 1-h bakeout at 150°C .

III. RESULTS AND DISCUSSION

A. Angular distributions

Figure 3 shows typical angular distributions for the $\langle 100 \rangle$ direction and the $\langle 110 \rangle$ direction both above and below the normal-incommensurate phase transition. A considerable effort has been concentrated on angular distribution measurements in the $\langle 100 \rangle$ direction at surface temperatures between 50 and 140 K. Within the experimental error all the main Bragg peak intensities show the same pure exponential decay with increasing temperature due to the Debye-Waller attenuation.

To estimate the corrugation amplitude, we perform an eikonal-approximation calculation using the corrugation function as given by Cantini.¹¹ Since no significant asymmetry in the angular distributions is observed, the second term in Cantini's corrugation function containing the deviation from the hexagonal symmetry was neglected keeping the following corrugation function:

$$\zeta(\mathbf{R}) = 2\zeta_0 \left[\cos \left[\frac{2\pi}{a}x \right] + \cos \left[\frac{2\pi}{a}y \right] + \cos \left[\frac{2\pi}{a}(y-x) \right] \right] \quad (1)$$

with $a = 3.44 \text{ \AA}$, the lattice vector of $2H\text{-TaSe}_2$. With this expression we obtained a fit of the data which is comparable to that achieved by Cantini *et al.* Our value of $\zeta_0 = 0.04 \pm 0.01 \text{ \AA}^{-1}$ is also very close to their value of 0.06 \AA^{-1} . We note, however, that in both cases some of

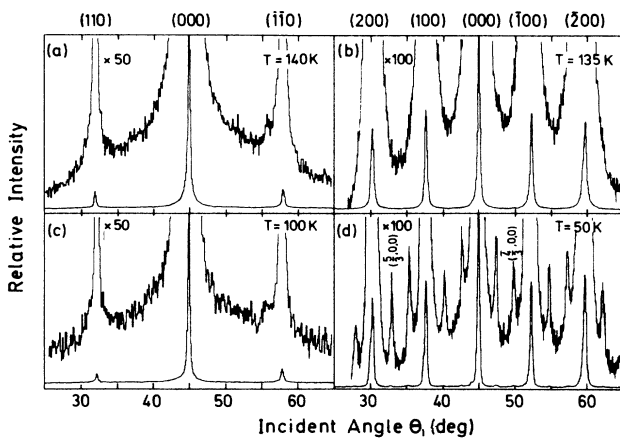


FIG. 3. Angular distributions of the intensity of scattered helium atoms in the $\langle 110 \rangle$ direction [panels (a) and (c)] and in the $\langle 100 \rangle$ direction [panels (b) and (d)]. Panels (a) ($T = 140 \text{ K}$) and (b) ($T = 135 \text{ K}$) are above the phase transition temperature T_0 , while panels (c) ($T = 100 \text{ K}$) and (d) ($T = 50 \text{ K}$) lie below T_0 . Each of the panels shows both an angular distribution with all of the peaks and also a magnified version of the angular distribution. In the magnified curves, the first-order superstructure peaks are clearly visible along $\langle 100 \rangle$ [panel (d)] where they have an amplitude at $T = 50 \text{ K}$ of $\sim 1\%$ of the main lattice peaks. In the $\langle 110 \rangle$ direction [panel (c)] no superstructure peak is observed below T_0 . The incident wave vector is $k_i = 11.5 \text{ \AA}^{-1}$ for the $\langle 110 \rangle$ direction and $k_i = 11.7 \text{ \AA}^{-1}$ for the $\langle 100 \rangle$ direction. All of the main Bragg peaks have been labeled along with two of the superlattice peaks which will be further discussed.

the large peaks are reproduced only to within a factor of 2. A better fit would probably be possible by using a realistic soft potential.

In the expanded curve of Fig 3(d), additional sharp peaks between the main lattice peaks are visible corresponding to the (3×3) superlattice formed by the three charge-density waves. These peaks are only visible in the $\langle 100 \rangle$ direction, whereas in the $\langle 110 \rangle$ direction only weak second-order superlattice peaks are expected [Fig. 3(c)].¹⁴ The intensities of the superstructure peaks are less than 1% of the main lattice peaks, indicating a very small additional corrugation induced by the formation of the charge-density waves below the transition temperature $T_0 = 122$ K. Therefore, only first-order peaks are observable in these experiments; however, the second-order peaks have been detected in neutron-scattering experiments.¹⁴ These superlattice peaks have a strong temperature dependence. Figure 4 shows some angular distributions for increasing temperatures, extending from the C phase ($T = 58$ K and 80 K) through the S ($T = 98$ K) and the I phase ($T = 119$ K) to the N phase ($T = 135$ K). Through all of these phases the intensity of the superlattice peaks decreases continuously with increasing temperature and becomes zero in the N phase. To account for the Debye-Waller attenuation of the superlattice peaks, we assume that it is described by the measured attenua-

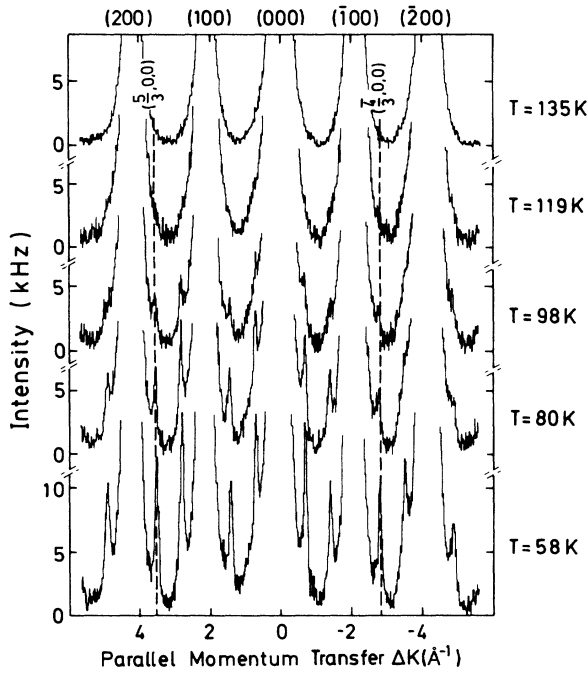


FIG. 4. A series of angular distributions showing the scattered intensity vs the parallel momentum transfer Δk in the $\langle 100 \rangle$ direction taken for increasing crystal temperatures. The scale is magnified, which cuts off the specular and the main Bragg peaks. Between the main lattice peaks $(m, 0, 0)$ the superstructure peaks are shown at $m \pm \frac{1}{3}$ positions; however, only two are labeled. At $T = 58$ K the intensity of the superstructure peak is about 1% of the main lattice diffraction peaks.

tion of the nearest main lattice peak. Thus the Debye-Waller effect can be approximately eliminated by taking the ratio of the areas under the maxima. The results for the $(-\frac{4}{3}, 0, 0)$ and the $(\frac{5}{3}, 0, 0)$ peaks are shown in Fig. 5. The superstructure peaks first appear below the critical temperature for the phase transition from the N to the I CDW phase ($T_0 = 122$ K).

The comparison between the integrated intensity normalized to the nearest Bragg peak for increasing and decreasing temperatures, as shown in Fig. 5, indicates a small amount of hysteresis in the temperature range $88 \leq T \leq 113$ K ($0.7 \leq T/T_0 \leq 0.9$). The existence of the S phase in this range for increasing crystal temperatures suggests that it is responsible for this difference. In this experiment only continuous intensity changes were observed, whereas in the neutron bulk data a discontinuous step was observed.¹⁴ However, the presence of the hysteresis strongly indicates a first-order phase transition for the commensurate-incommensurate phase transition. This is in agreement with the x-ray measurements of Fleming *et al.*³⁵ From the relative intensities of the superstructure peaks we derive the excess corrugation induced by the charge-density wave, ζ_{CDW} . According to the procedure derived by Cantini,¹¹ this is given, in the $\langle 100 \rangle$ direction, by

$$\zeta_{CDW} = |q_{m \pm 1/3, 0, 0}|^{-1} |S_{m \pm 1/3, 0, 0} / S_{m, 0, 0}|, \quad (2)$$

where $(m, 0, 0)$ denotes the normal lattice \mathbf{G} vectors and $(m \pm \frac{1}{3}, 0, 0)$ denotes the CDW-induced satellite \mathbf{G} vectors, immediately above and below $\mathbf{G} = (m, 0, 0)$;

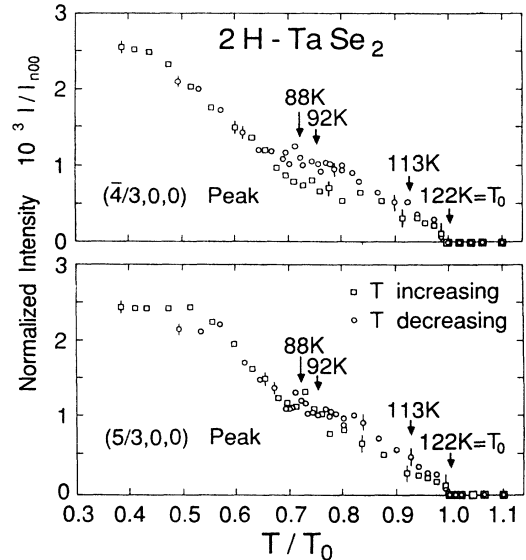


FIG. 5. Temperature dependence of the ratios of the intensities for the $(-\frac{4}{3}, 0, 0)$ and $(\frac{5}{3}, 0, 0)$ superlattice peaks relative to the closest Bragg peak intensities. The squares correspond to the normalized ratios for increasing temperature, the circles for decreasing temperature. Small hysteresis loops are seen around the S-I transition temperature (113 K), and in the region of the I-C (88 K) and the C-S (92 K) transitions.

$q_{m\pm 1/3,0,0}$ is the corresponding momentum transfer normal to the surface. The scattering amplitude S_G is related to the measured probability P_G by

$$P_G = e^{-2W_G} |S_G|^2 \tan \theta_i, \quad (3)$$

where θ_i is the incident angle for the corresponding diffraction peak (in our apparatus the sum of the incident and the final angle is 90°). The exponential term is the Debye-Waller factor, a slowly varying function of \mathbf{G} which approximately cancels out in the ratio of Eq. (2) and can, therefore, be neglected. The experimental results for the excess corrugation, derived from two of the most prominent satellites, $(\frac{5}{3}, 0, 0)$ and $(-\frac{4}{3}, 0, 0)$, are plotted in Fig. 6 as a function of the logarithm of $1 - T/T_0$ for both decreasing (left part) and increasing temperature (right part). The corrugation determined by Cantini¹¹ at 20 K (open circle) is seen to be in good agreement with the value extrapolated from our measurements.

For decreasing temperatures, but above the I - C transition, the excess corrugation can be well fitted by a straight line corresponding to a critical parameter $\beta = \frac{1}{3}$. However, the experimental error is such that a fitting with the mean-field value $\beta = \frac{1}{2}$ (Ref. 36) is also possible at temperatures close to the onset critical temperature T_0 . For increasing temperatures, the CDW amplitudes deviate from those for decreasing temperature due to the appearance of the striped phase between 92 and 113 K. Therefore, the extrapolation to $T = T_0$ is disturbed by the hysteresis of the I - S phase transitions and no critical exponent may be inferred. It is interesting to note that the value $\beta = \frac{1}{3}$ corresponds to that predicted for the (3D)- xy

(3D denotes three dimensional) model and is found in structural phase transitions of perovskites from cubic to tetragonal or to trigonal symmetry.³⁷ It also occurs in CDW systems, where the CDW amplitude serves as a two-component order parameter, e.g., in tetrathiafulvalene-tetracyanoquinodimethane (TTF-TCNQ) crystals.^{38,39} In these crystals, a CDW develops below 54 K through a second-order phase transition. The CDW is tridimensional, but the low-point symmetry of the lattice (C_{2n}) with a preferential direction implies a two-component order parameter and a second-order phase transition. The present results for $2H$ -TaSe₂ are indicative of a low-symmetry incommensurate CDW, namely they disagree with the earlier proposals of a hexagonal symmetry for the incommensurate phase stemming from x-ray analysis.³⁵ On the contrary, our data agree with the more recent direct observations of the incommensurate phase by microscopic techniques.^{12,30,40,41} In particular, Chen *et al.*³⁰ have found that the incommensurate phase on the cooling cycle does not show the hexagonal symmetry, as indicated by early x-ray-diffraction results, but instead, an orthorhombic symmetry on a microscopic scale (point group D_{2h}). The CDW-induced phase transition from the N to the C phase is structurally characterized in the bulk by a shift of the Se atoms in the z direction as determined by different methods to be 0.009 Å (Ref. 42) and 0.017 Å.¹⁴ For the surface layer, He-atom diffraction yields a value of 0.025 Å extrapolated to 0 K.^{10,11,43} In the case of the incommensurate structures there should be a small shift in the phase because of the incommensurability of the CDW wave vector. This small shift is not seen in our experiment because of the present resolution of about 1% at these incident energies for our apparatus.

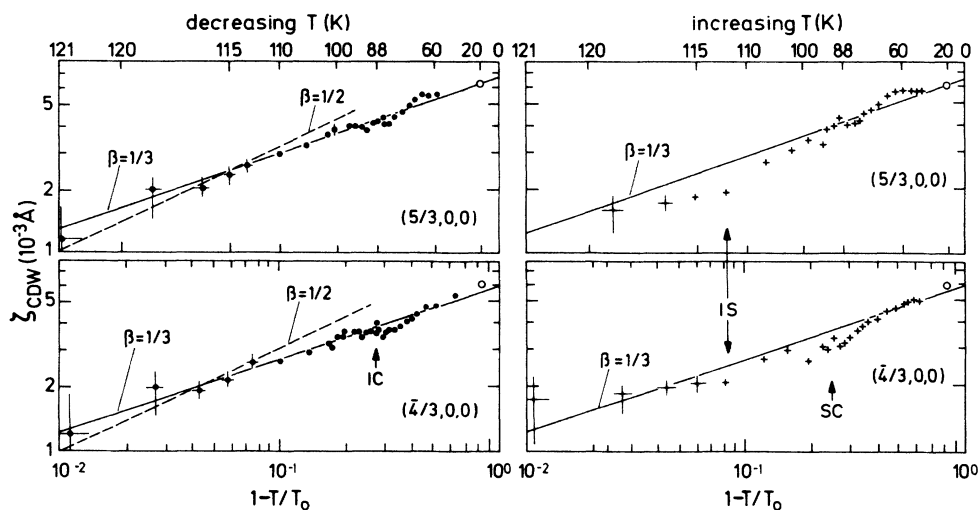


FIG. 6. Double-logarithmic plot of the charge-density-wave amplitude ζ_{CDW} vs $1 - T/T_0$ for the $(\frac{5}{3}, 0, 0)$ and $(-\frac{4}{3}, 0, 0)$ superstructure peaks for decreasing (left) and increasing (right) crystal temperature. The solid lines correspond to a slope $\beta = \frac{1}{3}$ and the dashed lines to the mean-field behavior ($\beta = \frac{1}{2}$). Arrows indicate the various phase-transition temperatures. The corrugation value obtained by Cantini (see Ref. 11) is shown as an open circle.

B. Time-of-flight spectra at $T = 140$ K

About 100 He-atom TOF spectra were measured for the normal phase of the $2H$ -TaSe₂ surface along the two high-symmetry directions of the surface Brillouin zone. Figure 7 shows a series of typical TOF spectra, which have been transformed to an energy scale. Each spectrum in Fig. 7 represents a 2-h measurement at constant incident angle θ_i , and constant target temperature $T = 140$ K. The initial beam energies were $E_i = 53.4$ and 71.5 meV, for the $\langle 110 \rangle$ and $\langle 100 \rangle$ directions, respectively. All spectra have a diffuse elastic peak and one or two low-energy phonon peaks which are attributed to the acoustic, transverse-polarized Rayleigh mode. In some of the spectra there are higher-energy peaks which are attributed to optical-phonon modes. The resulting dispersion curves are plotted in Fig. 8 and compared with Feldman's calculations of the bulk-phonon modes⁴⁴ based on the neutron data of Moncton *et al.*¹⁴ and Raman data on the optical modes.^{45–47} Overall, there is good agreement, except that the Rayleigh mode at the zone boundary is considerably lower than the corresponding Σ_3 acoustic bulk

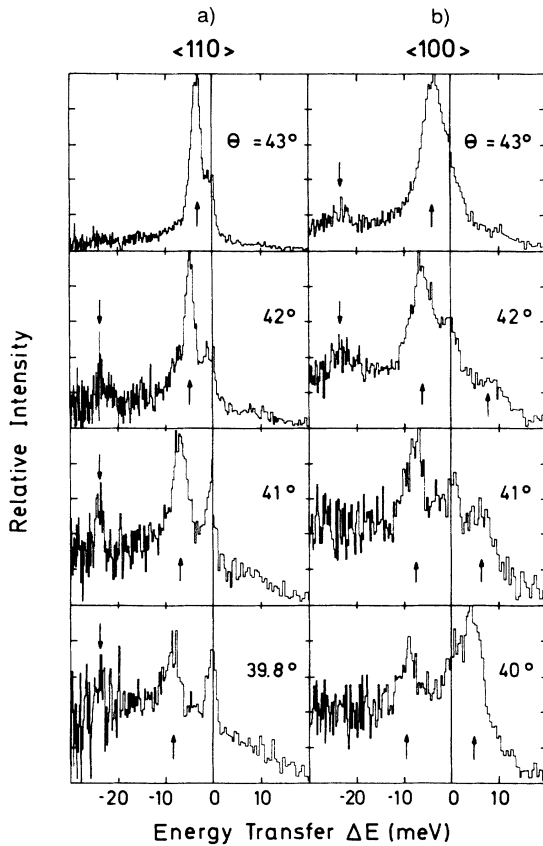


FIG. 7. Energy-transformed TOF spectra for $2H$ -TaSe₂(001) for several incident angles θ , at constant target temperature $T = 140$ K. (a) Incident energy $E_i = 53.4$ meV for the $\langle 110 \rangle$ direction, (b) incident energy $E_i = 71.5$ meV for the $\langle 100 \rangle$ direction. The arrows mark the phonon peaks; the peak at $\Delta E = 0$ corresponds to diffuse elastic scattering.

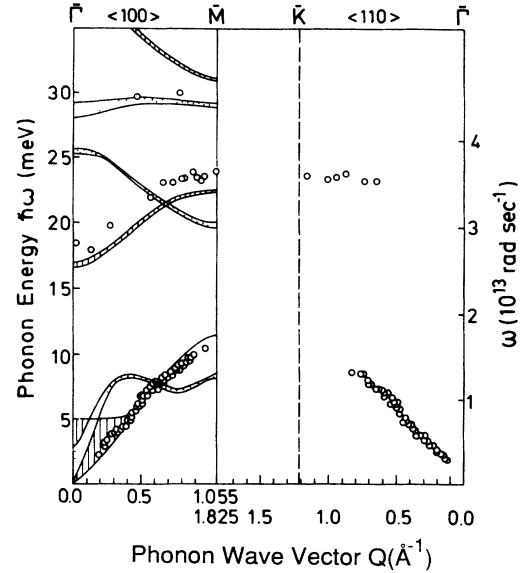


FIG. 8. Experimental data of the phonon modes along the border of the irreducible part of the surface Brillouin zone in the normal state ($T = 140$ K). The lattice-dynamical calculation by Feldman (Ref. 44) based on the fit of the available bulk data for the $\langle 100 \rangle$ direction is also included. Only those bands which have a component in the sagittal plane are plotted (striped area, Σ_3 symmetry; dotted area, Σ_1 symmetry).

band edge. A new fit of these data as well as of the available neutron and optical data, by means of the dispersive linear-chain (DLC) method,² is given in Sec. III D.

Along the $\langle 110 \rangle$ direction we were not able to measure the dispersion curve of the Rayleigh mode up to the Brillouin-zone boundary because the inelastic intensity was too low. Our data for this mode, which are also shown in Fig. 8, are limited to $Q \leq 0.85 \text{ \AA}^{-1}$, where it is in good agreement with the bulk-phonon data [which are available only for wave vectors $< 0.6 \text{ \AA}^{-1}$ (Ref. 14)]. Only one optical branch, at 23 meV , was detectable in the $\langle 110 \rangle$ direction.

C. Time-of-flight spectra at 60 K and temperature dependence of the Rayleigh mode

Phonon dispersion curves were also measured for the commensurate (3×3) phase at $T = 60$ K (Fig. 9, open squares) and were found to be nearly identical to those for the normal phase at $T = 140$ K (Fig. 9, solid dots). There is a small softening of the Rayleigh mode at 140 K with respect to the 60 -K measurements in the region $0.5 \leq Q \leq 0.6 \text{ \AA}^{-1}$. This wave-vector region has been previously studied in detail as a function of temperature.⁴⁸ As can be seen in Fig. 10(a), the greatest softening occurs at a wave vector of $Q_s \approx 0.53 \text{ \AA}^{-1}$ and $T \approx 110$ K. As shown in Fig. 10(b), the softening in the bulk is restricted to the longitudinal mode and occurs at $Q_b = 0.7 \text{ \AA}^{-1}$. If we assume that the anomaly is due to the Kohn-type mechanism, the different wave vector for the anomaly of the surface Rayleigh mode indicates that the

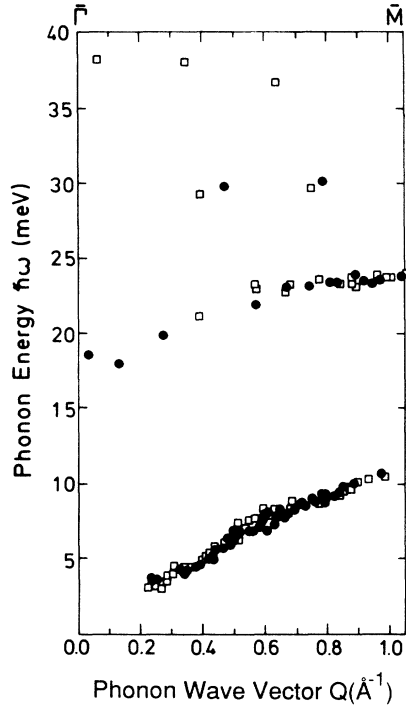


FIG. 9. Experimental data of the phonon modes along the $\Gamma\bar{M}$ ($\langle 100 \rangle$) direction at 140 K (solid circles) and 60 K (open squares). All data points, from energy loss and/or gain over the extended Brillouin zone, are included.

surface-electronic states at the Fermi energy have a wave-vector “nesting” at a different wave vector than the bulk electronic states.⁴⁸

Another possible explanation of the anomaly at $Q=0.53 \text{ \AA}^{-1}$ was a hybridization of the Rayleigh mode with a temperature-dependent surface longitudinal mode. Actually no distinct surface longitudinal mode was detected, presumably because of its lower excitation cross section as compared to the transverse Rayleigh mode. However, a series of TOF spectra taken at 60 K for slowly increasing θ_i suggests the presence of a weak double structure in the Rayleigh peak (Fig. 11) which we attribute to a crossing of the Rayleigh mode with a surface longitudinal mode. The frequencies of this mode, as deduced from this interpretation, are displayed in Fig. 12 (crosses) together with the other 60 K experimental points. From the data we can rather precisely determine the crossing of the two modes to occur at a wave vector of 0.6 \AA^{-1} . The crossing in the bulk is also observed at 0.6 \AA^{-1} (at 300 K) (Ref. 14) and not at 0.53 \AA^{-1} . At 60 K the minimum in the Σ_1 mode has about the same energy as at 300 K, namely about 7 meV, and therefore the surface longitudinal mode coincides, within the experimental error, with the bulk Σ_1 mode. Although it is expected that the crossing shifts towards lower Q values for temperatures closer to the normal-incommensurate phase-transition temperature, as can be argued from Fig. 10, a clear separation from the anomaly of the Rayleigh mode is still expected.

D. Dispersive linear-chain fit

The present experimental results include both acoustic and optical modes in TaSe₂. They provide the first measurements of the optical modes and although they might seem slightly softer than the corresponding bulk bands, they complement the existing room-temperature neutron data¹⁴ which have been obtained only in the acoustic region and the Raman data^{45–47} taken at $Q=0$ (Fig. 12, open circles). We have used the neutron, Raman, and our optical mode results with the dispersive linear-chain method to obtain a new fit to the bulk dispersion curves.

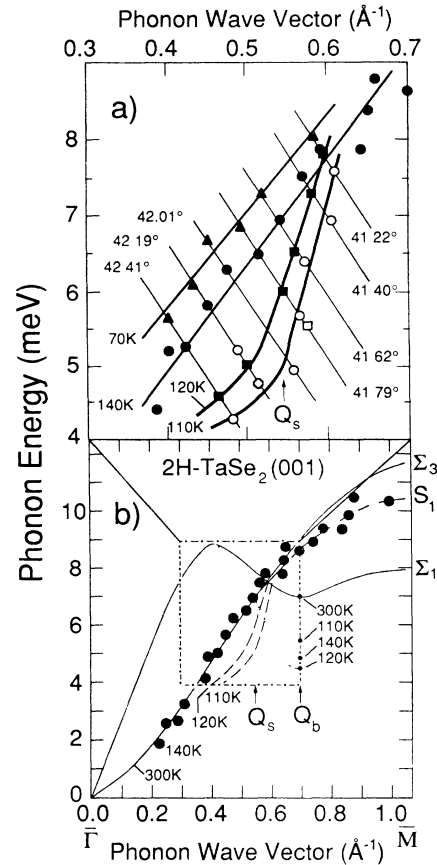


FIG. 10. (a) The temperature-dependent Rayleigh-mode dispersion over a limited Q -vector range (top scale), revealing the anomalous softening at $Q_s \approx 0.53 \text{ \AA}^{-1}$: solid circles, 140 K; solid squares, 120 K; open squares, 115 K; open circles, 110 K; lozenges, 100 K; triangles, 70 K. The interpolating thick solid lines are guides for the eye. The thin lines are the scan curves at different incident angles. (b) The experimental points (solid points) for the Rayleigh mode in $2H\text{-TaSe}_2(001)$ along $\langle 100 \rangle$ at 140 K. The solid lines are the transverse- (Σ_3) and longitudinal- (Σ_1) acoustic bulk modes (from Ref. 14). The dashed lines show the Rayleigh-mode (S_1) dispersion curve and its temperature-dependent anomaly for 110 and 120 K. For comparison, the temperature dependence of the bulk Σ_1 anomaly at $Q_b \approx 0.7 \text{ \AA}^{-1}$ is also shown (Ref. 14). The dotted line is our qualitative interpretation.

This calculation is described in a separate paper.⁴⁹ In Fig. 12 we compare the experimental data to the calculated bulk bands of Σ_3 and Σ_1 symmetries, having a polarization in the sagittal plane (the vertical striped area is for the shear vertical, and the oblique striped area for longitudinal polarization).

For the sake of clarity, we have reproduced only the 60-K He-atom scattering data (solid squares). They include three isolated high-energy points around 38 meV. The paucity of high-energy points can be explained by the fact that above 35 meV phonon peaks are hard to detect due to the weak intensity. Among all the TOF spectra, only three showed reliable peaks which determine the position of the upper branch in the fitting procedure of the bulk bands. A similar procedure has been used to fit the Rayleigh branch (heavy solid line) in order to infer the nature of the surface perturbation. The most salient feature in the bulk structure is the well-known deep anomaly in the bulk LA (Σ_1) band which goes below the bulk TA (Σ_3) band and the Rayleigh branch above $Q=0.6 \text{ \AA}^{-1}$.

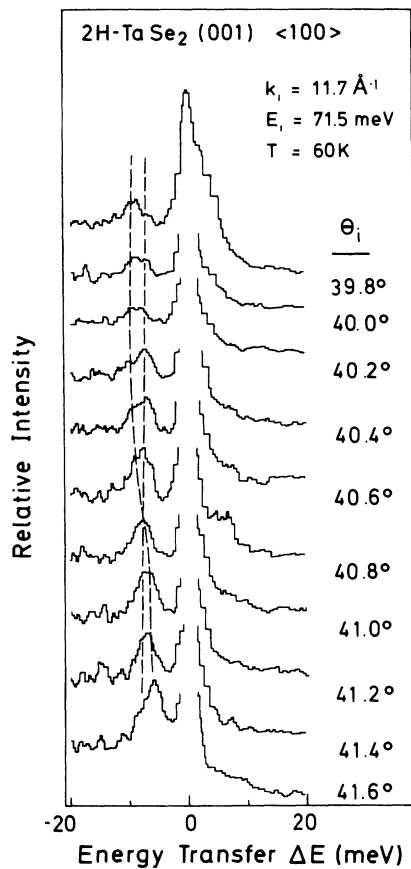


FIG. 11. Energy-transformed TOF-spectra for incident angles in the region of the crossing between a longitudinal-acoustic and the Rayleigh mode. The dashed lines suggest a double structure in the region where the shear-vertical Rayleigh mode and the longitudinal mode are hybridized and both are observable.

On the other hand, the Rayleigh branch shows a significant softening at the zone boundary. As discussed in Ref. 49, the surface perturbation responsible for such softening has to be concentrated in the Ta atomic sheet where an appreciable attraction is switched on presumably due to some rearrangement of the free-electron charge at the surface. A similar situation is found in the fitting of the longitudinal bulk bands, including the LA anomaly, which is consistent with the occurrence of a CDW instability in the gas of the conduction electrons in the Ta sheet.

Our fit, despite its simplicity, is consistent with the idea that all the anomalous behavior in $2H\text{-TaSe}_2$ comes from the Coulomb longitudinal interactions in the Ta plane, which are responsible for the CDW instability, in agreement with recent microscopic calculations.⁵⁰ Also, the temperature-dependent anomaly of the Rayleigh wave, appearing at one-half of the zone, around the CDW transition temperature, can be attributed to the same mechanism.⁴⁸ It is important to remark that the anomalies in the LA and Rayleigh modes may well be governed by the same mechanisms due to the surface-induced coupling between shear vertical and longitudinal components implied by elliptical polarization. As a consequence, the Σ_1 mode is observable in the crossing region around $Q=0.6 \text{ \AA}^{-1}$.

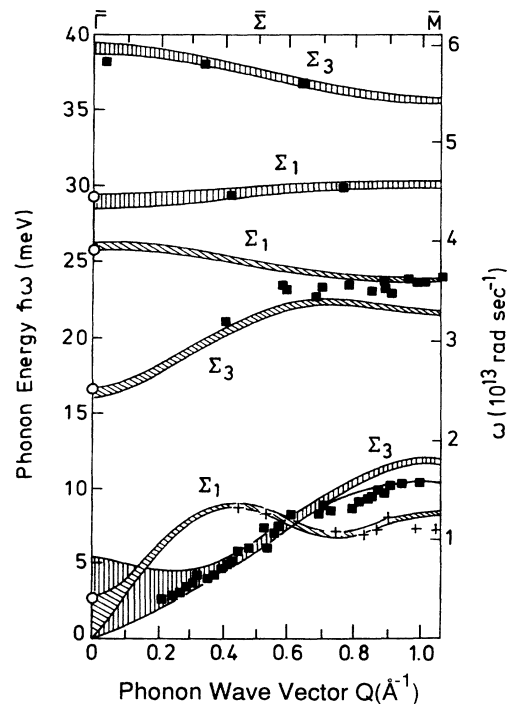


FIG. 12. Comparison of He-atom scattering data at 60 K (solid squares and crosses) and Raman data (open circles) for $2H\text{-TaSe}_2(001)$ surface in the $\langle 100 \rangle$ direction with the calculated bulk-phonon bands and the calculated Rayleigh branch (heavy solid line). The calculation is from the dispersive linear-chain method (Ref. 49).

IV. CONCLUSIONS

In this paper we have presented He-atom scattering studies of the structure and the dynamics of the $2H$ -TaSe₂(001) surface at various temperatures above and below the critical value T_0 for the CDW reconstruction. The intensity of the superstructure peaks increases continuously from zero as the temperature is lowered below $T_0 = 122$ K, indicating a second-order phase transition. The temperature dependence of the excess corrugation induced by the charge-density wave suggests a critical exponent $\beta = \frac{1}{3}$, but experimental uncertainties are such that the mean-field value $\beta = \frac{1}{2}$ cannot be ruled out. A small amount of hysteresis is found in the superstructure peak intensities in connection with the first-order I - C (S - C) and I - S phase transitions.

Our measured surface-phonon dispersion curves show that the Rayleigh-mode branch begins to fall below the bulk band near 0.7 \AA^{-1} and progressively decreases all the way out to the Brillouin-zone boundary. This observation has been interpreted by a simple model linking the surface perturbation to a force-constant change in the topmost Ta sheet.^{48,49}

A comparison of the surface-phonon dispersion curves measured at 140 K for the normal lattice with the measured phonon dispersion curve for the commensurate CDW phase at $T = 60$ K shows, in general, identical behavior. A deviation has only been detected for a small range of wave vectors between 0.4 and 0.6 \AA^{-1} . A careful study of the temperature dependence of the phonon energies for these relevant wave vectors reveals the existence of an anomaly at $Q \approx 0.53 \text{ \AA}^{-1}$ in the transverse-acoustic Rayleigh mode,⁴⁸ whereas the anomaly for the bulk longitudinal-acoustic branch is present at two-thirds of the zone. The latter is attributed to a Kohn-anomaly mechanism involving the conduction electrons of the Ta sheets⁴⁸ so that a change in the anomalous features for the surface region is consistent with our observations that the surface perturbation is concentrated in the topmost Ta sheet.

Ernst *et al.* have observed in W(001) a surface incom-

mensurate CDW which gradually locks into the substrate with decreasing temperature, until it drives a $c(2 \times 2)$ surface reconstruction.⁵¹ There seems to be a subtle analogy between W(001) and the surface behavior of TaSe₂(001) since, in both cases, one may speak of a competition between the surface, which contains internal stresses pulling towards a given (generally incommensurate) superstructure, and the bulk which works as a template and tends to lock the surface into a commensurate phase. The internal surface stress may originate from the fact that, in general, the surface-electronic state cuts the Fermi level at a wave vector k_{FS} different from the bulk k_F . For TaSe₂, this is inferred from the anomalous softening of the Rayleigh mode occurring both at around one-half and at the boundary of the Brillouin zone, whereas the bulk LA mode is softened at about two-thirds of the zone. Moreover, the anomaly minimum occurs somewhat below the bulk transition temperature T_0 , say about 110 K, at which temperature the S - I transition occurs when heating the crystal. Because of this correspondence, we are tempted to regard such a transition as triggered by the surface stress originating from an electron-phonon coupling at a $2k_{FS}$ different from the bulk $2k_F$.

ACKNOWLEDGMENTS

We are indebted to Dr. F. Levy (Ecole Polytechnique Fédérale de Lausanne) for providing the samples of $2H$ -TaSe₂, and we acknowledge discussions with J. R. Manson, E. Manousakis, and Y.-L. Wang. G.B., L.M., and J.G.S. acknowledge the hospitality of the Max-Planck-Institut (MPI) für Strömungsforschung in Göttingen. This work was supported in part by the North Atlantic Treaty Organization (NATO), Grant No. 571/83, by the U.S. Department of Energy (J.G.S.) through Grant No. DE-FG05-85ER45208, by the European Community under Contract No. ST2P-0013-1-F(CD), and by the Deutsche Forschungsgemeinschaft (Bonn, Germany) under Sonderforschungsbereich No. 126.

*Permanent address: Department of Physics, Florida State University, Tallahassee, Florida 32306-3016

¹G. Brusdeylins, R. Rechsteiner, J. G. Skofronick, J. P. Toennies, G. Benedek, and L. Miglio, *Phys. Rev. B* **34**, 902 (1986).

²L. Miglio and L. Colombo, *Phys. Rev. B* **37**, 3025 (1988).

³G. Benedek, G. Brusdeylins, C. Heimlich, J. P. Toennies, and U. Valbusa, *Surf. Sci.* **178**, 545 (1986).

⁴J. P. Toennies and R. Vollmer, *Phys. Rev. B* **40**, 3495 (1989).

⁵J. P. Toennies and R. Vollmer (unpublished).

⁶J. L. Wilkes, R. E. Palmer, and R. F. Willis, *J. Electron Spectr. Rel. Phenom.* **44**, 355 (1987).

⁷J. A. Wilson, F. J. DiSalvo, and S. Mahajan, *Adv. Phys.* **24**, 117 (1975).

⁸G. Brusdeylins, C. Heimlich, and J. P. Toennies, *Surf. Sci.* **211/212**, 98 (1989).

⁹P. Cantini, G. Boato, and R. Coella, *Physica B + C (Amsterdam)* **99B**, 59 (1980).

¹⁰P. Cantini and R. Coella, *Solid State Commun.* **53**, 77 (1985).

¹¹P. Cantini, in *Dynamics of Gas-Surface Interactions*, edited by G. Benedek and U. Valbusa (Springer-Verlag, Heidelberg, 1982), p. 84.

¹²R. V. Coleman, B. Drake, P. K. Hansma, and G. Slough, *Phys. Rev. Lett.* **55**, 394 (1985).

¹³G. Brusdeylins, F. Hofmann, P. Ruggerone, J. P. Toennies, R. Vollmer, G. Benedek, and J. G. Skofronick, in *Proceedings of the Third International Conference on Phonon Physics and Proceedings of the Sixth International Conference on Phonon Scattering in Condensed Matter, Heidelberg, 1989* (World Scientific, Singapore, in press).

¹⁴D. E. Moncton, J. D. Axe, and F. J. DiSalvo, *Phys. Rev. Lett.* **34**, 734 (1975); *Phys. Rev. B* **16**, 801 (1977).

¹⁵D. B. McWhan, J. D. Axe, and R. Youngblood, *Phys. Rev. B* **24**, 5391 (1981).

¹⁶L. Pfeiffer, R. E. Walstedt, R. F. Bell, and T. Kovacs, *Phys. Rev. Lett.* **49**, 1162 (1982).

¹⁷M. Naito and S. Tanaka, *J. Phys. Soc. Jpn.* **51**, 228 (1982).

- ¹⁸L. Pfeiffer, T. Kovacs, and F. J. DiSalvo, *Phys. Rev. Lett.* **52**, 687 (1984).
- ¹⁹G. K. Scott, K. K. Bardhan, and J. C. Irwin, *Phys. Rev. Lett.* **50**, 771 (1983).
- ²⁰R. M. Fleming, D. E. Moncton, J. D. Axe, and G. S. Brown, *Phys. Rev. B* **30**, 1877 (1984).
- ²¹C. W. Chu, L. R. Testardi, F. J. DiSalvo, and D. E. Moncton, *Phys. Rev. B* **14**, 464 (1976).
- ²²C. W. Chu, V. Diatschenko, C. Y. Huang, and F. J. DiSalvo, *Phys. Rev. B* **15**, 1340 (1977).
- ²³J. M. E. Harper, T. H. Geballe, and F. J. DiSalvo, *Phys. Rev. B* **15**, 2943 (1977).
- ²⁴R. A. Craven and S. F. Meyer, *Phys. Rev. B* **16**, 4583 (1977).
- ²⁵J. A. Wilson, F. J. DiSalvo, and S. Mahajan, *Phys. Rev. Lett.* **32**, 882 (1974).
- ²⁶M. Barmatz, L. R. Testardi, and F. J. DiSalvo, *Phys. Rev. B* **12**, 4367 (1975).
- ²⁷M. O. Steinitz and J. Grunzweig-Genossar, *Solid State Commun.* **29**, 519 (1979).
- ²⁸W. G. Herrenden-Harker, in *Charge-Density-Waves in Solids*, Vol. 217 of *Lecture Notes in Physics*, edited by Gy. Hutiray and J. Solyom (Springer-Verlag, Berlin, 1985).
- ²⁹J. A. Wilson and R. Vincent, *J. Phys. C* **17**, 123 (1984).
- ³⁰C. H. Chen, J. M. Gibson, and R. M. Fleming, *Phys. Rev. B* **26**, 184 (1982).
- ³¹T. Onozuka, N. Otsuka, and H. Sato, *Phys. Rev. B* **34**, 3303 (1986).
- ³²G. Brusdeylins, R. B. Doak, and J. P. Toennies, *Phys. Rev. B* **27**, 3662 (1983).
- ³³G. Benedek, L. Miglio, J. G. Skofronick, G. Brusdeylins, C. Heimlich, and J. P. Toennies, *J. Vac. Sci. Technol. A* **5**, 1093 (1987).
- ³⁴Abelestik Laboratories, 833 West 182nd Street, Gardena, CA 90248.
- ³⁵R. M. Fleming, D. E. Moncton, D. B. McWhan, and F. J. DiSalvo, *Phys. Rev. Lett.* **45**, 576 (1980).
- ³⁶L. D. Landau and E. M. Lifschitz, *Statistische Physik I* (Akademie-Verlag, Berlin, 1984), p. 148.
- ³⁷K. A. Muller and W. Berlinger, *Phys. Rev. Lett.* **26**, 13 (1971).
- ³⁸P. Bak, *Physica B + C* (Amsterdam) **99B**, 325 (1980); *Rep. Prog. Phys.* **45**, 587 (1982).
- ³⁹R. H. Friend and D. Jerome, *J. Phys. C* **12**, 1441 (1979).
- ⁴⁰K. K. Fung, S. McKernan, J. W. Steeds, and J. A. Wilson, *J. Phys. C* **14**, 5417 (1981).
- ⁴¹Y. Koyama, Z. P. Zhang, and H. Sato, *Phys. Rev. B* **36**, 3701 (1987).
- ⁴²J. A. Wilson, *Phys. Rev. B* **17**, 3880 (1978).
- ⁴³G. Brusdeylins, C. Heimlich, J. G. Skofronick, J. P. Toennies, R. Vollmer, and G. Benedek, *Europhys. Lett.* **9**, 563 (1989).
- ⁴⁴J. L. Feldman, *Phys. Rev. B* **25**, 7132 (1982).
- ⁴⁵J. A. Holy, M. V. Klein, W. L. McMillan, and S. F. Meyer, *Phys. Rev. Lett.* **37**, 1145 (1976).
- ⁴⁶J. E. Smith, Jr., J. C. Tsang, and M. W. Shafer, *Solid State Commun.* **19**, 283 (1976).
- ⁴⁷J. C. Tsang, J. E. Smith, Jr., and M. W. Shafer, *Solid State Commun.* **27**, 145 (1978).
- ⁴⁸G. Benedek, G. Brusdeylins, C. Heimlich, L. Miglio, J. G. Skofronick, J. P. Toennies, and R. Vollmer, *Phys. Rev. Lett.* **60**, 1037 (1988).
- ⁴⁹G. Benedek, L. Miglio, G. Brusdeylins, C. Heimlich, J. G. Skofronick, and J. P. Toennies, *Europhys. Lett.* **5**, 253 (1988).
- ⁵⁰K. Motizuki, K. Kimura, E. Ando, and N. Suzuki, *J. Phys. Soc. Jpn.* **53**, 1078 (1984).
- ⁵¹J. Ernst, E. Hulpke, and J. P. Toennies, *Phys. Rev. Lett.* **58**, 1941 (1987).